The adsorption of silane, disilane and trisilane on polycrystalline silicon : a transient kinetic study

ELSEVIER

Surface Science 367 (1996) 321–339

surface science

The adsorption of silane, disilane and trisilane on polycrystalline silicon: a transient kinetic study

W.L.M. Weerts[1], M.H.J.M. de Croon, G.B. Marin *

Laboratorium voor Chemische Technologie, Eindhoven University of Technology, P.O. Box 513, 5600 MB Eindhoven, The Netherlands

Received 21 January 1996; accepted for publication 20 June 1996

Abstract

The adsorption of silane, disilane and trisilane on polycrystalline silicon was investigated using temporal analysis of products (TAP) following on admission of a reactant pulse in the temperature range 300–1000 K and at pressures typical for low-pressure chemical vapour deposition. Up to 650 K a slow adsorption process is operative for the three silanes. A quantitative description of the adsorption in this temperature range is possible with a mechanism based on an insertion reaction of the silanes into surface hydrogen bonds. Above 650 K a much faster mode of adsorption is observed, which for the higher silanes is accompanied by silane formation. Homogeneous gas-phase reactions can be excluded. Silane adsorption above 820 K can be described quantitatively with a dual-site adsorption mechanism.

Keywords: Adsorption kinetics; Chemisorption; Models of surface kinetics; Molecule–solid reactions; Silane; Silicon; Surface chemical reaction

1. Introduction

In the recent past the adsorption and concomitant surface reaction pathways of the silanes SiH_4, Si_2H_6 and Si_3H_8 have been investigated using techniques such as temperature-programmed desorption (TPD) coupled to static secondary ion mass spectrometry (SSIMS) (e.g. [1,2]), laser-induced thermal desorption (LITD) [3,4], modulated molecular beam scattering (MMBS) [5,6] and reflection high-energy electron diffraction (RHEED) [7]. These studies all have been performed under UHV conditions on well-defined single-crystalline surfaces.

Direct information about adsorption and subsequent surface reactions of silanes on less well-defined silicon surfaces such as amorphous and polycrystalline silicon is scarce. Indirect information mostly is based on LPCVD growth data. Buss et al. [8] studied the adsorption of silane and disilane on polycrystalline silicon using molecular beam scattering (MBS) in the temperature range 900–1350 K. A simple mechanism was proposed to explain the observations: a dissociative adsorption of silane and disilane with competing associative desorption of silane and further dehydrogenation of the silicon hydride species to solid silicon and dihydrogen. A reasonable agreement between model and experiment was found.

In the present study, an alternative method to

* Corresponding author. Fax: +31 40 2446653.

[1] Present address: Philips CFT, Eindhoven, The Netherlands.

PII S0039-6028(96)00876-X

investigate adsorption and surface reactions of silanes on polycrystalline silicon is chosen. The temporal analysis of products (TAP) technique [9] was used to provide direct information about the kinetics and the mechanism of the surface steps. Substrate growth rates were not measured. The elucidation of the kinetics of the reactions that produce solid films from SiH_4, Si_2H_6 and Si_3H_8 on polysilicon substrates was achieved by monitoring the transient responses of the above silanes after introduction of pulses into a specially designed silicon-wafer stacked reactor. Only one similar TAP study on CVD precursors is known in the literature [10]. In the latter, the pyrolysis of trimethylantimony and tetramethyltin is investigated. However, in contrast to the present work, no real, planar substrates were used for the deposition in the reactor, but supposedly inert quartz granules, implying that the pyrolysis was assumed to occur by gas-phase decomposition. In our study, gas-phase reactions were excluded as far as possible in order to focus on surface reactions.

The relatively high reactivity of the silanes used towards adsorption on polysilicon, and even on fully hydrogenated polysilicon, permitted a very large temperature regime from room temperature up to about 1000 K in the TAP experiments. The quality of the data, however, becomes less reliable at high temperatures, due to the large consumption of the silanes. Above about 900 K, the conversion of the silanes in the reactor approaches 100%. In principle both TAP and MMBS can provide the same information about adsorption and surface reactions of silanes, with about the same time resolution for the determination of kinetic parameters. MMBS, however, is a high vacuum technique, whereas the pressure conditions under which TAP experiments are performed are close to the conditions of low-pressure chemical vapour deposition (LPCVD). This indeed makes TAP a means to bridge the gap between the high vacuum conditions of surface science and the real world of CVD.

2. Experimental

2.1. Apparatus

All experiments were conducted using a temporal analysis of products (TAP) set-up which has been described in detail elsewhere [9]. Only the key features relevant to the present work are given here. The principal components of the TAP set-up include (i) a gas feed system that supplies reactants to two high-speed pulse valves and a continuous flow valve, (ii) a microreactor, (iii) three interconnected vacuum chambers that house the microreactor valve assembly and the quadrupole mass-spectrometer detector, and (iv) a Hewlett-Packard Series 360 computer workstation. Mass spectrometry is used to follow outlet responses towards pulses of reactants admitted at the inlet with a sub-millisecond time resolution.

The TAP microreactor, valves for introduction of the gas pulses, and a solenoid valve for introduction of a continuous flow of reactant gas are located in the reactor vacuum chamber, with vacuum being supplied from a Varian VHS10 oil diffusion pump and a Varian SD700 mechanical pump. Typical background pressures in this chamber are in the range 10^{-5}–10^{-4} Pa. The differential chamber is located between the reactor vacuum chamber and the analytical chamber. Vacuum in the differential chamber is provided by a Varian VHS6 oil diffusion pump with a liquid nitrogen trap, with secondary vacuum being supplied from a Varian SD700 mechanical pump. Vacuum in the analytical chamber, containing the ionisation head of the UTI 100C quadrupole mass spectrometer, is provided by a Balzers TPU450H turbo-molecular pump together with a Balzers MD4TC diaphragm pump. The pressures in the differential and analytical chambers are usually 10^{-6} and 10^{-7} Pa, respectively.

2.2. Microreactor

The microreactor developed for the present work can be considered as a batch wise-operated reactor. Indeed, the reactants are admitted in typically 200 μs, which can be considered instantaneous compared to a typical residence time of 20 ms. The square Inconel microreactor with an inside diameter of 0.434 cm and an overall length of 4.72 cm was charged with seven Si(100) wafers. The wafers are placed at equal distances of 278 μm from each other. This ensures Knudsen diffusion for gas pulse intensities up to 3×10^{15} molecules per pulse. The

reactor temperature is monitored using a type-K thermocouple located half-way between the fourth and fifth wafer. For proportional-integral-derivative (PID) temperature control, a second type-K thermocouple is positioned in the reactor wall. As a consequence of the low pressure inside the reactor vacuum chamber, significant axial temperature gradients exist over the wafers. At 300 K the total temperature difference across the wafers is negligible; at 1000 K, however, it amounts to about 50 K. Therefore the temperatures reported with the experiments were obtained by temperature averaging across the wafers. Moreover, pulse injection results in total pressure non-uniformity in the axial direction. Fig. 1 illustrates the evolution of a typical calculated pressure profile following a pulse injection. This profile was obtained by solving numerically the continuity equation for the gas phase under isothermal conditions, as discussed in Section 4.1.

2.3. Materials

Argon (99.999%, Hoek Loos), a mixture of helium, neon, argon, krypton and xenon (20% each, Air Products), silane (99.999%, Air Products), disilane (99.99%, Air Products), trisilane (99.28%, Solkatronic), hydrogen (99.999%, Hoek Loos), and deuterium (99.8%, Hoek Loos) are used. Pure trisilane and binary gas mixtures of silane/disilane and argon are used as feed gases for the pulse transient experiments. Argon serves as reference component for determination of the pulse size and calculation of the effective Knudsen diffusion coefficient of the other reactant gas. Hydrogen is used for pretreatment of the deposition surface. Deuterium is admitted to monitor deuterated desorption products from the surface.

Double-side polished (100) n-type silicon wafers with a resistivity of $\sim 0.015\ \Omega \cdot$cm and an average thickness of 302 μm are cleaved into small rectangular slices with dimensions 0.4 and 3.0 cm, and placed inside the microreactor. Prior to each series of experiments the slices and reactor walls are purged with hydrogen at 1100 K and coated with approximately 1000 monolayers of undoped polycrystalline silicon at 900 K. Possible effects of a thin native oxide layer, present in spite of the hydrogen pretreatment, are eliminated during the initial stages of the deposition run. The adsorption

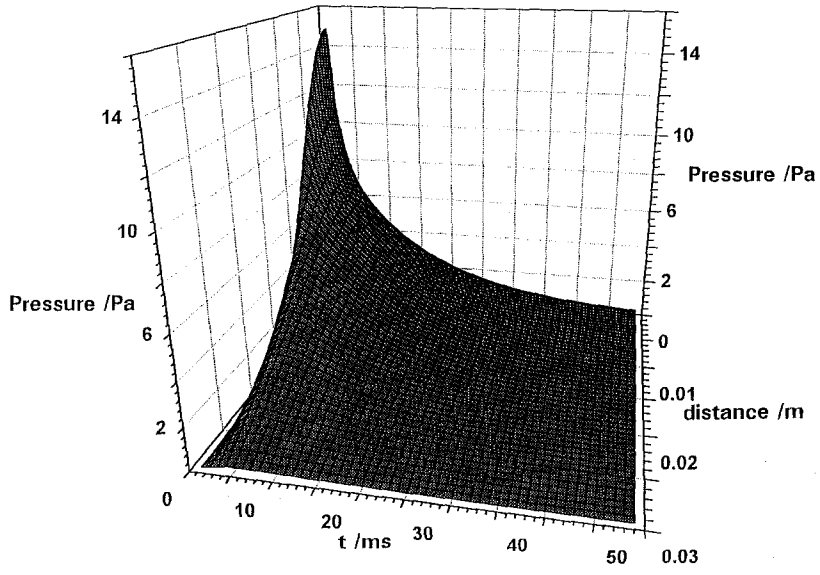

Fig. 1. Calculated evolution of the pressure profile in the TAP reactor after introduction of an argon pulse at $t=0$ s at the entrance of the wafer stack of length 3 cm with a distance between the wafers of 278 μm. Pulse size 2.05×10^{14} molecules, $T=462$ K, $D_{K,eff,Ar} = 1.37 \times 10^{-2}\ m_g^3\ m_r^{-1}\ s^{-1}$.

capacity, i.e. the maximum amount of molecules that can be adsorbed on the reactor walls and the wafers, is about 1.5×10^{16}.

2.4. Procedures

Experiments are conducted using both the scan and pulsed modes of operation, reported in detail elsewhere [9]. In a typical scan experiment, a continuous flow of a reactant gas or mixture is introduced to the microreactor, and the mass spectrum of the effluent gases is measured in the range 1–150 amu at various increasing temperatures. Scan experiments are used for determination of the fragmentation patterns of the pure reactant gases, as well as for tracing and identification of important reaction products formed in the microreactor.

Key fragments of the above mentioned silanes are present at amu (atomic mass unit) values of 30, 60 and 85. The main peak of silane occurs at 30 amu, while those of disilane and trisilane coincide at 60 amu. Prior to the adsorption experiments the purity of the silane used was checked with respect to disilane. Disilane content typically proved to be less than 0.01%. During the pulse experiments, silane is monitored at 30 amu, disilane at 30 and 60 amu and trisilane at 30, 60 and 85 amu, whereas hydrogen and argon are followed at 2 and AMU 40 amu, respectively. Due to the low pumping efficiency for molecular hydrogen, it is not considered possible to make a quantitative analysis of this surface-generated product.

In a typical pulsed mode experiment, the pulse valve driver and reactant pressure are adjusted to produce the desired gas pulse intensity. The quadrupole mass spectrometer (QMS) is then set to an appropriate amplifier range and mass center for a given mass to charge value. Pulse, multipulse and alternating pulse experiments can be distinguished.

During a *pulse* experiment, the raw output signal from the QMS is sampled at a minimum time increment of 10 μs over a minimum sampling period of 0.1 s to produce a maximum of 10 000 points per pulse. Provided the pulse shape does not change from pulse to pulse, subsequent pulses, admitted to the microreactor at a user-specified time interval called the repetition time, are signal averaged to improve the signal-to-noise ratio. In most cases, before pulse averaging, at least ten pulses are needed to obtain a stable response signal as required for pulse averaging. A normalized response curve can be obtained by dividing the TAP response curve by its value at peak maximum.

During a *multipulse* experiment, a specified number of pulses is given during a specified time interval. No signal averaging is applied in order to visualize the intensity change occuring in a pulse train.

In an *alternating pulse* experiment, reactants are introduced in an alternating sequence using the two high-speed pulse valves. The valves are fired simultaneously or in sequence, separated by a specified time-interval. The data collection window for the quadrupole mass spectrometer is set in such a way that both pulses are recorded in the same output response. Signal averaging is applied to improve the signal-to-noise ratio.

The determination of an absolute callibration factor for argon is done by means of experiments with the continuous flow valve. With known argon/silane and argon/disilane mixtures, it then is possible to obtain calibration factors for both silanes. The absolute calibration factors allow conversion of the dimension of the QMS signal into flow rates in moles per second. Knowing the input pulse intensity of a reactant and integrating its outlet molar flow rate function over time enables the conversion of the reactant in the reactor to be calculated.

TAP responses can be calculated by integrating the appropriate continuity equations analytically or numerically (vide infra). In this work, the numerical integration is used during the estimation of parameters with a single response regression routine [11]. The parameters consist of effective diffusion coefficients and reaction rate coefficients. The regression consists of obtaining maximum likelihood estimates for the parameters by application of the least-square criterion to the observed and calculated molar flow rates at the reactor outlet. The objective function used is based upon the assumption that experimental errors are normally distributed with zero mean. The significance of the global regression is expressed by means of the so-called "F ratio", which is based on the ratio of

the mean calculated sum of squares to the mean regression sum of squares [12]. The significance of the parameter estimates was tested by means of their approximate t values. These approximate t values were used to determine the 95% confidence intervals reported in the present work.

For trisilane, no good calibration of the pulse intensity could be obtained as pure trisilane was used; so in this case the total amount of pulsed gas N_p is treated as an extra parameter and is estimated with the above parameter-estimation method. It should be noted that, at least for linear processes, pulse intensity is not important in kinetic parameter estimation. The highest binary correlation coefficient between estimated pulse size and other parameters used for the modelling of trisilane responses amounts to 0.91.

For all responses it was also necessary to estimate a delay time t_0. This parameter corresponds to the time interval between the triggering of the valve actuator and the opening of the pulse valve. Included in it is also the mean time delay needed for molecules to travel from the reactor outlet to the quadrupole. In all experiments, a delay time of about 1.2 ms is found. It was verified that the estimated delay times correspond to the values observed experimentally.

3. Qualitative results

3.1. Adsorption of silane

Pulse experiments with a mixture of 20% argon in silane are performed in the temperature range 300–1000 K with pulse intensities between 1×10^{15} and 1×10^{16} molecules per pulse, i.e. up to roughly the adsorption capacity of the reactor. Typical results are shown in Fig. 2. Up to 820 K a rather low and constant conversion of about 18% of silane is observed, indicating only slightly activated chemisorption. Above this temperature the conversion rises sharply from 18% at 820 K to 76% at 850 K, indicating a shift in the dominant adsorption mechanism.

Analogue continuous flow experiments show no evidence for gaseous products formed during the chemisorption, except for hydrogen. In addition, alternating pulse experiments in which the surface is pretreated with deuterium prior to the admittance of silane do not show formation of deuterated silanes.

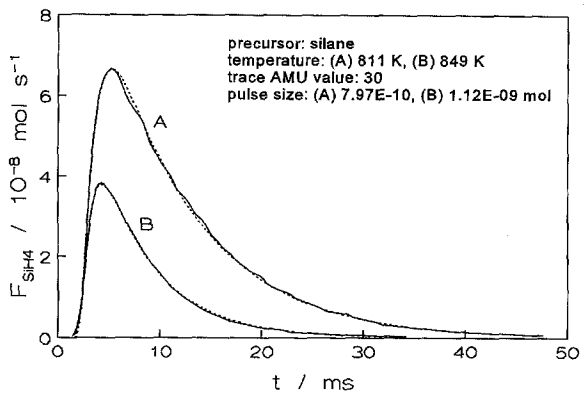

Fig. 2. Silane molar flow rates at outlet of reactor versus time at (A) 811 and (B) 849 K. Full lines: experimental. Dashed line (A): calculated using Eqs. (9) and (2)–(4) and the estimated parameters listed in Table 1. $N_{p,SiH4}=7.97\times10^{-10}$ mol, $D_{K,eff,SiH4}=1.80\times10^{-2}$ m_g^3 m_r^{-1} s^{-1}. Dashed line (B): calculated using Eqs. (11)–(17) and the estimated values $(1-\theta^o_{H*})=0.316$ and $t_o=1.20\times10^{-3}$ s. $N_{p,SiH4}=1.12\times10^{-9}$ mol; $D_{K,eff,SiH4}=1.90\times10^{-2}$ m_g^3 m_r^{-1} s^{-1}, $k_a=37\,776$ m_g^3 mol^{-1} s^{-1}.

Multipulse experiments in the temperature region below 820 K show non-changing response shapes for over 200 silane pulses, which is indicative of an unaltered adsorption surface during the experiment. In the high-temperature region multipulse experiments are rather difficult to reproduce, whereas signal heights increase steadily during the multipulse sequence. Up to 60 pulses are needed to obtain a steady signal for the silane response. The conversion of silane also increases considerably in this temperature region. A more quantitative discussion of silane adsorption at high temperatures will be given in Section 4.3.

3.2. Adsorption of higher silanes

3.2.1. Trisilane

Pulse experiments with pure trisilane in the temperature region up to 710 K show a rather low conversion of trisilane, increasing from about 18% at 300 K to almost 35% at 710 K, which is indicative of a slightly activated chemisorption

reaction for trisilane in this region. Fig. 3a shows the normalized response signals of 30, 60 and 85 amu measured during a pulse experiment performed at 648 K. The fact that all response signals coincide indicates that formation of silane and disilane are not found. Multipulse experiments with pure trisilane performed in the same temperature region reveal equal response shapes over more than 100 pulses, indicative of a non-changing adsorption surface. Moreover, deuterium/trisilane alternating pulse experiments, in which the surface is pretreated with deuterium prior to the admittance of trisilane, show no formation of deuterated trisilane nor of deuterated silicon-containing products.

Above 710 K a second chemisorption reaction of trisilane is observed, leading to considerably higher conversions of trisilane. Fig. 3b again shows the normalized response signals of 30, 60 and 85 amu, but now for a pulse experiment with pure trisilane performed at 846 K. The abundance of the 30 amu response signal compared to the coinciding 60 and 85 amu response signals provides direct evidence for the presence of silane formation and the absence of disilane formation. The maximum of the silane outlet molar flow rate occurs at approximately 1×10^{-2} s, and the maximum of the trisilane outlet molar flow rate at 5×10^{-3} s. The question now arises if silane is formed through heterogeneous or through homogeneous decomposition of trisilane. Homogeneous decomposition of trisilane into silane and silylsilylene is possible on the time scale of a typical pulse experiment (10^{-2} s), as may be calculated using the Rice–Ramsperger–Kassel–Marcus (RRKM) theory. The corresponding unimolecular reaction rate coefficient [13], calculated by taking into account wall-effects, amounts to 78 s^{-1} at 850 K and 100 Pa, giving rise to a characteristic reaction time of 1.3×10^{-2} s, which indeed is comparable to the time scale of a pulse experiment.

Evidence for the heterogeneous decomposition of trisilane into silane, however, is obtained from Fig. 4, showing the overall 30 amu response signal, i.e. originating from both trisilane and formed silane, as a function of pulse intensity at 797 K. The response signals A–D clearly consist of two peaks, one positioned at roughly 4×10^{-3} s and corresponding to the 30 amu response signal of trisilane, and another located between 1×10^{-2} and 5×10^{-2} s reflecting the 30 amu response signal of the formed silane. If normalized with respect to the main silane 30 amu response signal at about 0.005 s, the relative importance of the second 30 amu signal located between 0.01 and 0.05 s clearly increases with decreasing pulse intensity, going from response signal A to D, and hence with decreasing total pressure. This effect is opposite to that expected on the basis of the RRKM theory, meaning that the silane leaving the microreactor is formed at the surface during the chemisorption of trisilane, and not via unimolecular decomposition of trisilane in the gas phase.

Fig. 4 also shows that the amount of formed silane, reflected by the surface area of the corresponding 30 amu response signal, is independent of trisilane pulse intensity for response signals A–D. This implies that the number of sites available for trisilane adsorption is independent of the number of admitted trisilane molecules.

Fig. 5 shows the trisilane 60 amu and the overall 30 amu response signals as a function of the temperature. The trisilane 60 amu response signal decreases with increasing temperature from 772 K (A) to 869 K (D). At 944 K, all trisilane is converted. The corresponding response signal (not shown) coincides completely with the time axis. The faster the adsorption with increasing temperature, the shorter the mean residence time of the trisilane molecules. This is caused by the greater adsorption probability of the trisilane molecules with a larger residence time, leading to less tailing. At 772 K normalization of the trisilane 60 amu and the overall 30 amu response signals, similar to the case depicted in Fig. 3b, demonstrates the presence of a small amount of formed silane. An increase in temperature from 772 to 819 K shows a decrease in the trisilane 60 amu response signal with a concomitant increase in the overall 30 amu response signal, indicative of more silane formation at higher temperature. By increasing the temperature from 819 to 846 K, more silane is formed. Then, going from 846 to 944 K, the overall 30 amu response signal considerably reduces in height and exhibits a strong narrowing. This points to adsorption of the silane formed upon the adsorption of

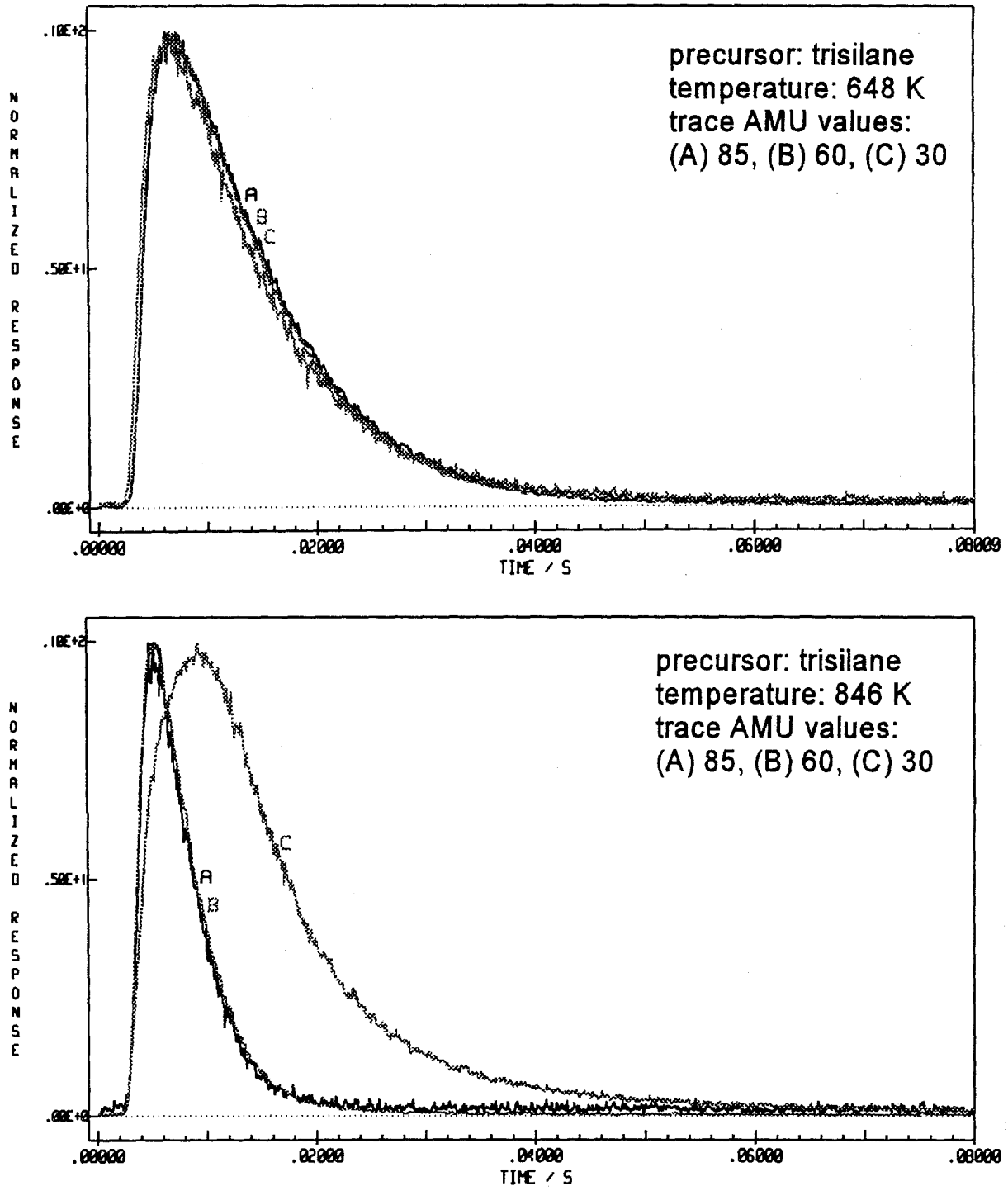

Fig. 3. Normalized response signals of (A) 85, (B) 60 and (C) 30 amu during a pulse experiment with pure trisilane at (a) 648 and (b) 846 K.

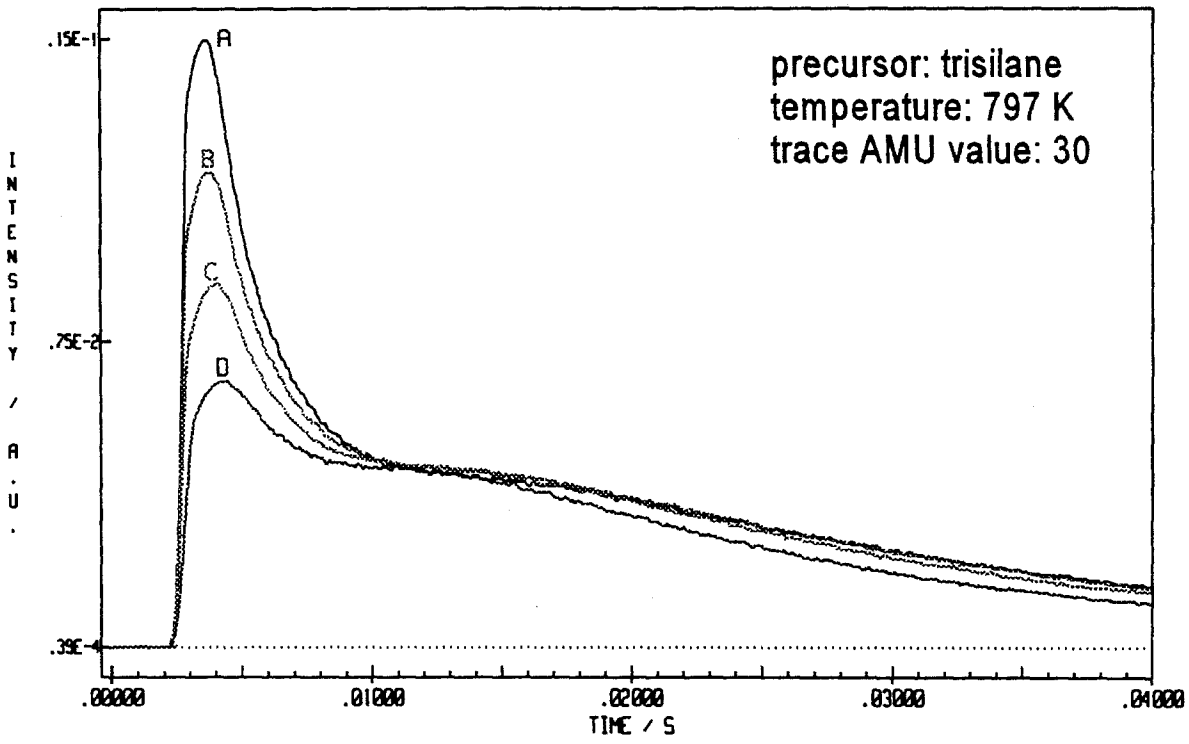

Fig. 4. Overall 30 amu response signal, originating from both trisilane and formed silane, as a function of pulse intensity during pulse experiments with pure trisilane at 797 K. Pulse intensity decreases from A to D.

trisilane. At 944 K the overall 30 amu response signal originates wholly from silane, as all trisilane has been converted at this temperature.

In the literature it is generally agreed that the adsorption processes of silane and trisilane are not or only slightly activated. Reported activation energies for silane adsorption range between 0 and 17 kJ mol^{-1} [8,14,15], whereas Gates [16] obtained a negative activation energy for trisilane adsorption of -21 kJ mol^{-1}. The strong effect of temperature on the trisilane and formed silane responses outlined above most probably can be attributed to a strongly activated surface process responsible for the partial regeneration of the hydrogenated silicon surface in the time intervals between subsequent pulses. An increase in temperature from 772 to 819 K consequently results in an increase in the number of vacant surface sites at the beginning of the pulses, and hence in an increase in the number of converted trisilane and formed silane molecules. At these temperatures, the number of vacant surface sites is probably too small to additionally permit adsorption of the formed silane. Around 846 K the onset of silane adsorption can be detected, considering the narrowing of the overall 30 amu response signal denoted by (C). A further increase in temperature towards 944 K results in an even faster regeneration of vacant surface sites in the time intervals between the pulses, leading to an enhanced adsorption of silane, and hence to a decrease in the number of silane molecules reaching the outlet of the microreactor. Note that almost all of the admitted trisilane molecules are converted at these high temperatures.

3.2.2. Disilane

Pulse experiments with a gas mixture of 20% argon and 80% disilane in the temperature range 300–900 K using pulse intensities from 1×10^{15} to

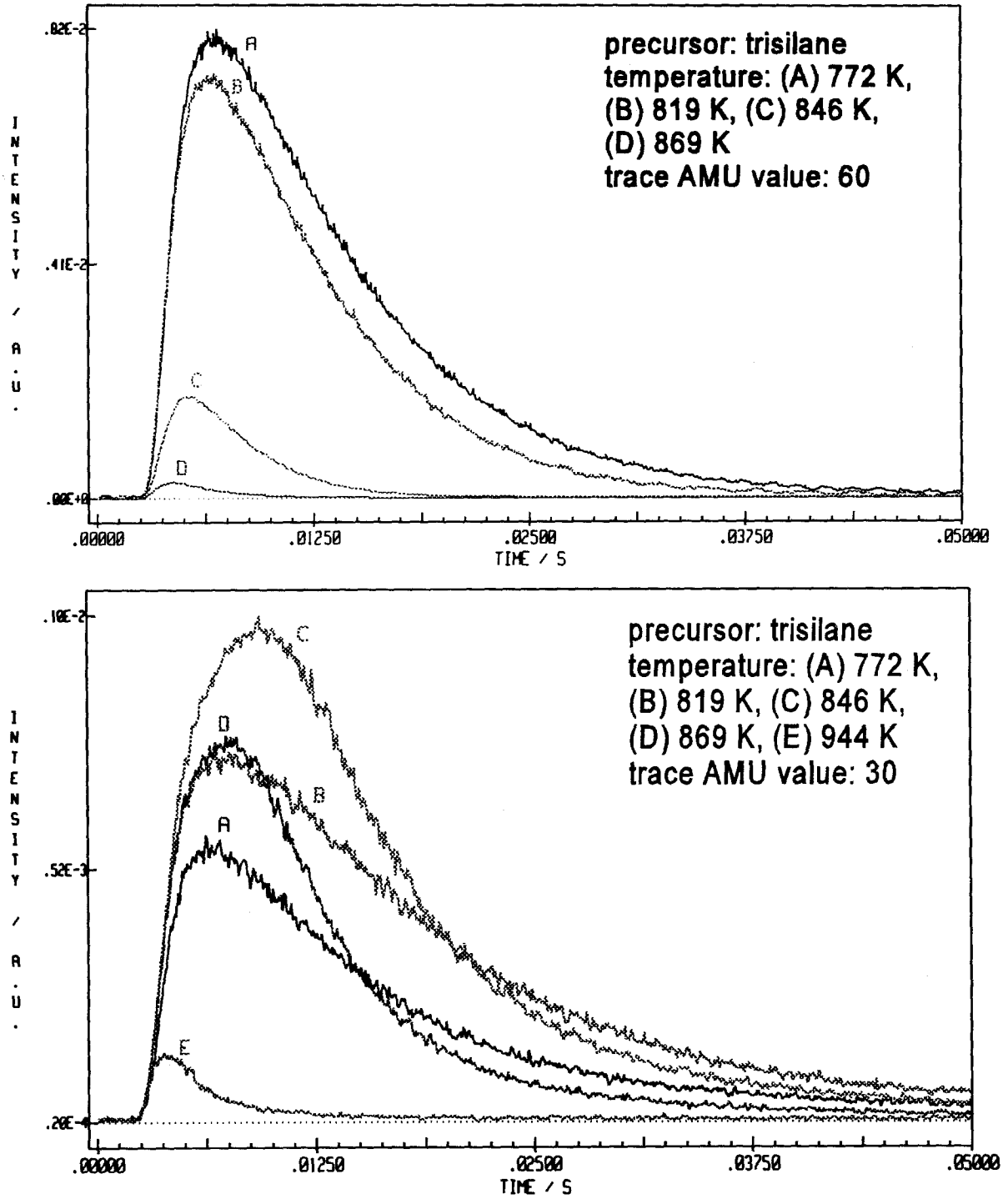

Fig. 5. (a) Trisilane 60 amu response signal and (b) overall 30 amu response signal, originating from both trisilane and formed silane, as a function of temperature during pulse experiments with pure trisilane at fixed pulse intensity. (A) $T=772$ K, (B) $T=819$ K, (C) $T=846$ K, (D) $T=869$ K, (E) $T=944$ K.

1×10^{16} molecules per pulse revealed similar results to those reported above for trisilane. In the temperature region up to 640 K a rather constant disilane conversion of roughly 25% can be derived from an overall silicon balance, indicating that the chemisorption of disilane is only slightly activated. As in the case of trisilane, no silane formation is observed in this low-temperature region. Deuterium/disilane alternating pulse experiments, in which the surface is pretreated with deuterium prior to the admittance of disilane, do not show any significant response signals of deuterated silicon-hydride species. Moreover, multipulse experiments reveal equal response shapes over more than 100 pulses in the same temperature region, indicative of a non-changing adsorption surface.

Above 640 K another chemisorption reaction of disilane is observed, producing silane in the gas phase. The considerably higher disilane conversion in this temperature region points to a shift in activation energy to much higher values. The question again arises as to whether silane is formed through heterogeneous or through homogeneous decomposition of disilane. With the RRKM theory a unimolecular reaction rate coefficient equal to 13.4 s^{-1} can be calculated for gas-phase decomposition of disilane into silane and silylene at 100 Pa and 850 K [13]. Comparison of the resulting characteristic reaction time, 7.5×10^{-2} s, with the time scale of a pulse experiment, 10^{-2} s, does not allow exclusion of homogeneous silane formation. However, evidence for the heterogeneous formation of silane is obtained from Fig. 6, showing the overall 30 amu response signal, originating from both disilane and formed silane, as a function of pulse intensity at 821 K. With decreasing pulse intensity going from response signal A to E, the maximum of the peak shifts to larger time values. This indicates that the overall 30 amu response signal is mainly caused by the desorption of silane, and not by the fragmentation of disilane in the quadrupole mass spectrometer. In the latter case the peak maximum of the presented 30 amu response signal would shift in the opposite direction, in exactly the same way as the response signals completely representative of the non-converted disilane. The formation of larger amounts of silane at lower pulse intensities, i.e. at lower total pressures, eliminates the possibility of homogeneous silane formation, since gas-phase decomposition of disilane will be faster at higher pressures.

Similar temperature effects as those shown in Fig. 5 on the response signals representative of trisilane and formed silane are observed in the disilane/argon pulse experiments performed at various temperatures above 640 K. Upon increasing the temperature, the response signal representative of formed silane first increases, then reaches its maximum value at about 650 K, and finally decreases.

4. Quantitative results and discussion

4.1. Experiments with inert gas

An inert isothermal gas mixture can be transported through the reactor by various mechanisms, such as viscous flow, molecular diffusion and Knudsen diffusion. At sufficiently high pressures, i.e. at pulse intensities above 2×10^{17} molecules per pulse, viscous flow will dominate. At sufficiently low pressures, i.e. at pulse intensities below 5×10^{15} molecules per pulse, diffusional transport will be predominant [17]. As at low pressures molecular diffusion coefficients are much larger than Knudsen diffusion coefficients, molecular diffusion in gas mixtures can be neglected. A pulsed-mode experiment involves total pressures of many orders of magnitude: relatively high pressures at the reactor inlet in the beginning of the pulse, low pressures at the reactor outlet (see Fig. 1). To verify that the gas transport is fully determined by Knudsen diffusion, the effective diffusion coefficient has to be determined as a function of pulse intensity. In the case of Knudsen diffusion, this coefficient has to show a square-root dependence on temperature and an inverse square-root dependence on the molar mass of the molecule under consideration.

In the case where diffusion is the controlling mechanism of gas transport and no reaction occurs, the continuity equation under isothermal conditions for a gas-phase component A in the reactor

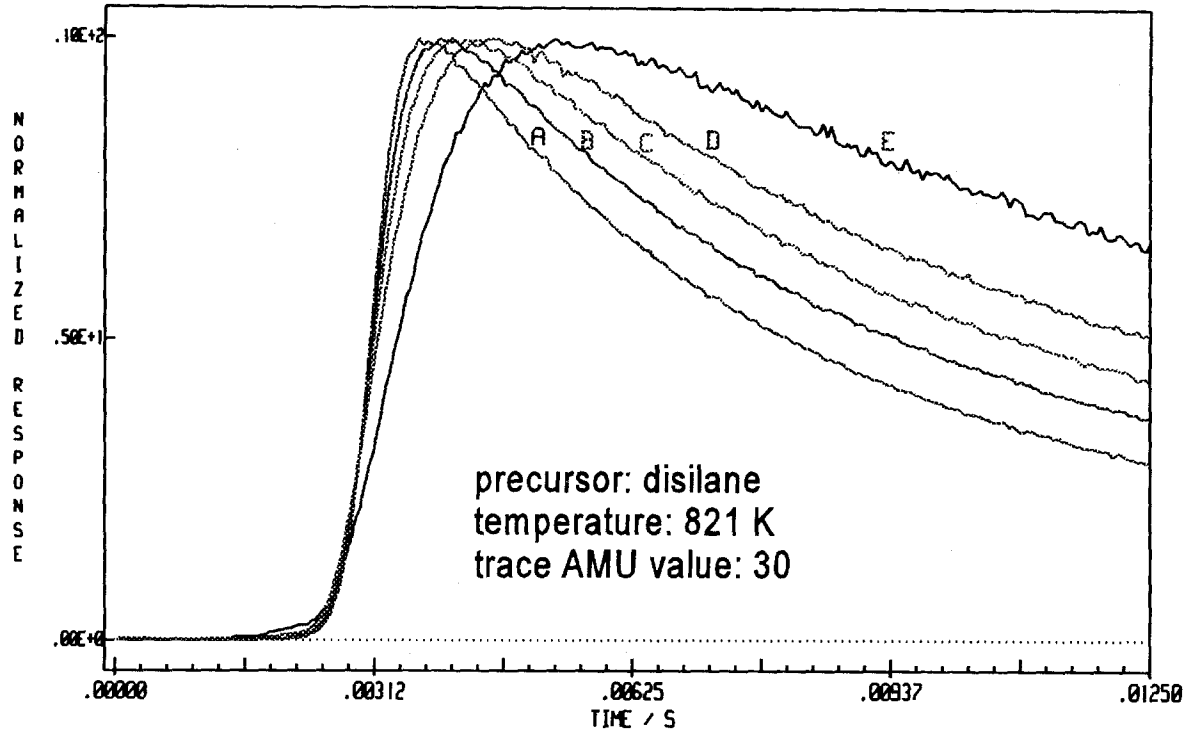

Fig. 6. Normalized overall 30 amu response signal, originating from both disilane and formed silane, as a function of pulse intensity during pulse experiments with a mixture of 20% Ar and 80% disilane at 821 K. Relative pulse intensities: (A) 6.0, (B) 5.0, (C) 3.5, (D) 2.5, (E) 1.0.

is given by

$$\epsilon \frac{\partial C_A}{\partial t} = D_{\text{eff,A}} \frac{\partial^2 C_A}{\partial x^2}, \tag{1}$$

where C_A is the gas concentration of component A (mol m_g^{-3}), ϵ is the porosity of the stack in the reactor ($m_g^3\ m_r^{-3}$), and $D_{\text{eff,A}}$ is the effective diffusion coefficient of A ($m_g^3\ m_r^{-1}\ s^{-1}$). Eq. (1) has to be solved using the following initial and boundary conditions [17]:

$$t = t_0 \wedge 0 \leq x \leq L \quad C_A = \delta_x \frac{N_{\text{p,A}}}{\epsilon A_s}, \tag{2}$$

$$t \geq t_0 \wedge x = 0 \quad \frac{\partial C_A}{\partial x} = 0, \tag{3}$$

$$t \geq t_0 \wedge x = L \quad C_A = 0. \tag{4}$$

Here $N_{\text{p,A}}$ is the inlet pulse size of component A (mol), A_s the cross-sectional area of the reactor (m_r^2) and L the stack length (m_r). Eq. (2) specifies that the initial gas concentration profile in the reactor is a delta function, which is a good approximation as long as the time scale on which the inlet pulse is admitted is much smaller than the time scale of the experiment. Other initial conditions are conceivable [18], but Eq. (2) is the easiest to implement both in the analytical and in the numerical solution of the continuity equation. Moreover, calculations of molar flow rates using various initial conditions indicate only minor differences between them, which are mostly within experimental error. The first boundary condition Eq. (3) implies the absence of flux at the reactor inlet when the pulse valve is closed. The second boundary condition Eq. (4) specifies that the reactor outlet is kept at vacuum conditions. The molar flow rate of component A, F_A, at the outlet of the reactor (mol s^{-1}), i.e. at $x = L$, is given by

$$F_A|_{x=L} = -D_{\text{eff,A}} A_s \left.\frac{\partial C_A}{\partial x}\right|_{x=L}. \tag{5}$$

Eqs. (1)–(5) can be integrated analytically, leading to a series expansion of the molar flow rate of A at the reactor outlet as a function of time [13,17]. Alternatively it can be solved numerically using the NAG Fortran Library routine D03PGF [19]. This routine integrates a set of nonlinear parabolic differential equations in one space variable by the method of lines and Gear's method. The partial differential equations are approximated by a set of ordinary differential equations obtained by replacing the space derivatives by finite differences. This set is integrated forwards in time using the method of Gear. The approximation applies a uniform user-specified grid in the space direction, whereas the time intervals are chosen by the routine. The routine does not allow a δ-function for the initial gas concentration profile such as given in Eq. (2). Therefore the initial gas concentration at the first and second discrete space points are set to some value C_A^0. In this way, Eq. (3) is satisfied at $t=t_0$. The gas concentration at the third and following grid points are taken to be zero. The value of C_A^0 is given by

$$C_A^0 = \frac{2N_{p,A}}{3\epsilon A_s \Delta x}, \tag{6}$$

with Δx denoting the distance between two successive grid points (m_r). A comparison between analytically and numerically calculated molar flow rates for various sets of parameters shows that they agree within 0.25% at all time points if at least 100 spacial grid points are applied.

Single-pulse experiments with an inert gas mixture of helium, neon, argon, krypton and xenon were performed with total pulse intensities from 5×10^{14} up to 1×10^{16} molecules per pulse. Knudsen-type diffusion was confirmed experimentally by reducing the inlet gas-pulse intensity until the normalized output responses of each component no longer changed as a function of the pulse intensity. This was found to occur at intensities lower than approximately 3×10^{15} molecules per pulse. The numerical model was used for the estimation of effective diffusion coefficients, as discussed in Section 2.4.

Fig. 7 presents the results from the experiments in which various inert inlet gases are pulsed through the wafer-stacked microreactor at a total pulse intensity of 1×10^{15} molecules per pulse and at $T=312$ K. Estimated effective diffusion coefficients are shown versus the reciprocal square root of the molar mass. A linear dependence, as expected for Knudsen diffusion, is observed. Similar experiments in which argon is pulsed while the reactor temperature is varied between 313 and 841 K show the expected square-root dependence of the effective diffusion coefficient on the temperature.

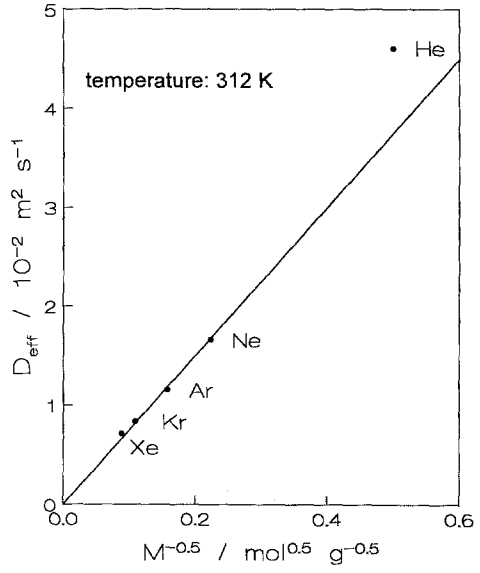

Fig. 7. Estimated effective diffusion coefficients for various inert gases as a fucntion of the reciprocal square root of their molar masses. Pulse size: 1.0×10^{15} molecules per pulse, $T=312$ K.

The above results indicate that at sufficiently low pulse intensities, thus at pulse sizes below 3×10^{15} molecules, Knudsen diffusion is the dominant mechanism of gas transport in the wafer-packed TAP microreactor. In principle the effective Knudsen diffusion coefficient might be calculated from

$$D_{K,eff,A} = \frac{\epsilon}{\tau_{stack}} D_{K,A}, \tag{7}$$

with ϵ and τ_{stack} the porosity and tortuosity of the wafer packed microreactor. $D_{K,A}$, the Knudsen diffusion coefficient ($m_g^2\ s^{-1}$), is given by

$$D_{K,A} = 2/3 h f_1(w/h) f_2(h/L) \sqrt{\frac{8RT}{\pi M_A}}, \tag{8}$$

with h the distance between two wafers in the stack, w the width of the wafer and L the length of the wafer. R, T and M_A have their usual meaning. The function $f_1(w/h)$ corrects for the effect of non-circular cross-section as given by Eldridge and Brown [20]. The function $f_2(h/L)$ corrects for the finite length of the microreactor, as discussed by Clausing [21]. Introduction of both corrections leads to calculated values of $D_{K,eff}$ for argon which only are equal to the measured values if τ_{stack} is set at about 4. Thus the calculated values of $D_{K,eff,A}$ are much larger than those deduced from the responses, as for the wafer-packed microreactor a tortuosity τ_{stack} of 1 is expected. Coronell and Jensen [22] simulated transition regime flow in a horizontal LPCVD reactor by means of a Monte Carlo method. The obtained Knudsen diffusion coefficients were a factor of nine lower than expected from Eq. (8) without the correction function f_2 (h/L). It was argued that the notion of a Knudsen diffusion coefficient in the interwafer geometry is ill-defined, since the diffusing molecules are not completely confined by the wafer as is the case in axial diffusion through an infinite tube. Clausing stated that the function f_2, deduced for a finite cylindrical tube only, is a very crude approximation. A better understanding of Knudsen flow in finite-length, non-cylindrical tubes should be a subject of further study. For the present purposes, however, it is sufficient to have shown the linear relation between the effective diffusion coefficients in the wafer-packed TAP microreactor, and the square root of the temperature and the reciprocal square root of the molar masses of the gases used. In this way it is possible to calculate effective diffusion coefficients for all gases in a mixture at an arbitrary temperature, knowing only one at a given temperature.

4.2. *Adsorption of silanes at low temperatures*

The qualitative experiments outlined in Section 3 revealed a weak temperature dependence for all three silanes in the low-temperature region, which may be attributed to adsorption kinetics [8,16]. Moreover, in the same region the surface was found to have a constant composition even after 100–200 pulses, i.e. after the adsorption of at least several monolayers. For example, 200 pulses of silane at a conversion of 16% correspond to the adsorption of 10 monolayers considering a mean pulse size of 5×10^{15} molecules per pulse and the adsorption capacity of the microreactor being equal to 1.5×10^{16} molecules. This is not much of a problem as long as the reactions after the adsorption step are so fast that in the time interval between two pulses, which is mainly of the order of a second, the free surface can be regenerated. It is known, however, that hydrogen desorption, whether first-order as on Si(001) [3,4,23–26] or second-order as on Si(111) [4], is a slow process with a characteristic time of about 1 s even at 850 K. This is consistent with the results obtained by Holleman and Verweij [27] and by Weerts [13]. These kinetic modelling studies showed that the desorption of molecular hydrogen from the hydrogenated polysilicon surface occurs with a similar characteristic time.

From the above considerations it can be inferred that the silicon surface used in the low-temperature TAP experiments is almost completely saturated with hydrogen. Adsorption processes will therefore not take place at vacant surface sites, but have to occur at hydrogen-covered sites. This implies that adsorption most probably occurs via an insertion reaction, e.g. for silane

$$Si(s)-H+SiH_4 \rightarrow Si(s)-SiH_3+H_2.$$

Since in the low-temperature region the reactivity towards adsorption is about equal for all three silanes, as can be deduced from the experimental conversions, similar reactions are postulated for the higher silanes

$$Si(s)-H+Si_2H_6 \rightarrow Si(s)-Si_2H_5+H_2,$$

$$Si(s)-H+Si_3H_8 \rightarrow Si(s)-Si_3H_7+H_2.$$

With Knudsen diffusion as the predominant mode of gas transport, the mass balance for all three silanes becomes

$$\epsilon \frac{\partial C_i}{\partial t} = D_{K,eff,i} \frac{\partial^2 C_i}{\partial x^2} - a_v L_t k_{ins} C_i, \tag{9}$$

which is subjected to the initial and boundary conditions given by Eqs. (2)–(4). Here, k_{ins} denotes

the adsorption/insertion rate coefficient. The disappearance term on the right-hand side of this equation features no dependency of the coverage of hydrogen-covered sites. It implies a constant and uniform adsorption surface during the pulse experiment. Complete desorption of hydrogen from the formed, presumably very unstable, compounds up to monohydride species will indeed result in a surface with the same amount of active Si–H sites for all three silanes at the beginning of each pulse. However, this need not necessarily be true, as can be inferred from literature on plasma-free CVD growth of hydrogenated amorphous silicon layers [28]. These layers were grown in the same temperature region in which the TAP experiments have been performed. The data support a hydrogen content in the bulk of the layer of 7 at% for trisilane and of about 5 at% for disilane, both at 673 K, implying that probably not all secondary hydrogen atoms desorb during the growth process. The figures may suggest small changes in the available number of adsorption sites, i.e. of Si–H sites at or near the surface, for the various silanes. However, it is questionable whether secondary hydrogen atoms on adsorbed higher silanes are sterically available as adsorption sites. Static SIMS measurements on Si(111)-(7 × 7) show that adsorbed SiH species are the primary stable species after exposure of the silicon surface to disilane in the temperature region of interest [2]. From time-of-flight direct reactivity measurements of the surface hydrogen coverage on Si(100) during chemical beam epitaxy (CBE) growth of silicon from SiH_4 and Si_2H_6 [29], about constant surface hydrogen/silicon atom ratios were obtained at low temperatures, although for Si_2H_6 the ratio proved not to be 1.0 but 1.5. These measurements give evidence for a constant number of adsorption sites, as requested by the above-stated model. Pulse experiments with a binary gas mixture of 20% argon and 80% silane performed in the temperature range 462–850 K were modelled using the above-mentioned equations. The effective Knudsen diffusion coefficient of silane was obtained from that of argon by correcting the latter by the appropriate square-root inverse ratio of the corresponding molar masses. This approach reduces the total number of unknown parameters to be estimated. Here, the adsorption/insertion rate coefficient k_{ins} and the zero time t_0 were estimated using the parameter estimation method as outlined in Section 2.4.

Fig. 2 (curve A) shows a typical comparison between an experimental and a calculated silane response. The experimental response applies to a pulse experiment performed at 811 K. Clearly, an excellent agreement between experiment and model is observed. Table 1 lists the corresponding parameter estimates with their 95% confidence intervals. The parameter estimates are not strongly correlated, the highest binary correlation coefficient amounting to 0.85.

Simulation of the same silane response with these parameter estimates yields a silane conversion equal to 18.6%. Fig. 8a shows an Arrhenius diagram of the adsorption/insertion rate coefficient k_{ins} obtained by regression of silane response data in the temperature range between 462–850 K. Clearly, two regimes can be distinguished with a transition occurring at a temperature of about 820 K.

Pulse experiments with binary gas mixtures of 80% disilane and 20% argon, and with pure trisilane performed in the temperature range 365–755 K, and from 388 up to 762 K, respectively, were also modelled. The effective Knudsen diffusion coefficients of disilane were obtained from the corresponding argon response signals as outlined earlier. The effective Knudsen diffusion coefficients of trisilane, on the other hand, were calculated by interpolation of the effective Knudsen diffusion coefficients of argon obtained from the silane and disilane experiments using the square-root dependence on temperature over molar mass.

Figs. 8b and 8c show the Arrhenius diagrams of the adsorption/insertion rate coefficients for disi-

Table 1
Parameter estimates with their approximate individual 95% confidence intervals obtained by regression of a silane response at 811 K using $D_{K,eff,SiH4} = 1.80 \times 10^{-2}$ m_g^3 m_r^{-1} s^{-1}; $N_{p,SiH4} = 7.97 \times 10^{-10}$ mol

Parameter	Estimate
k_{ins} (10^2 m_g^3 mol^{-1} s^{-1})	1.98 ± 0.06
t_0 (10^{-3} s)	1.15 ± 0.01

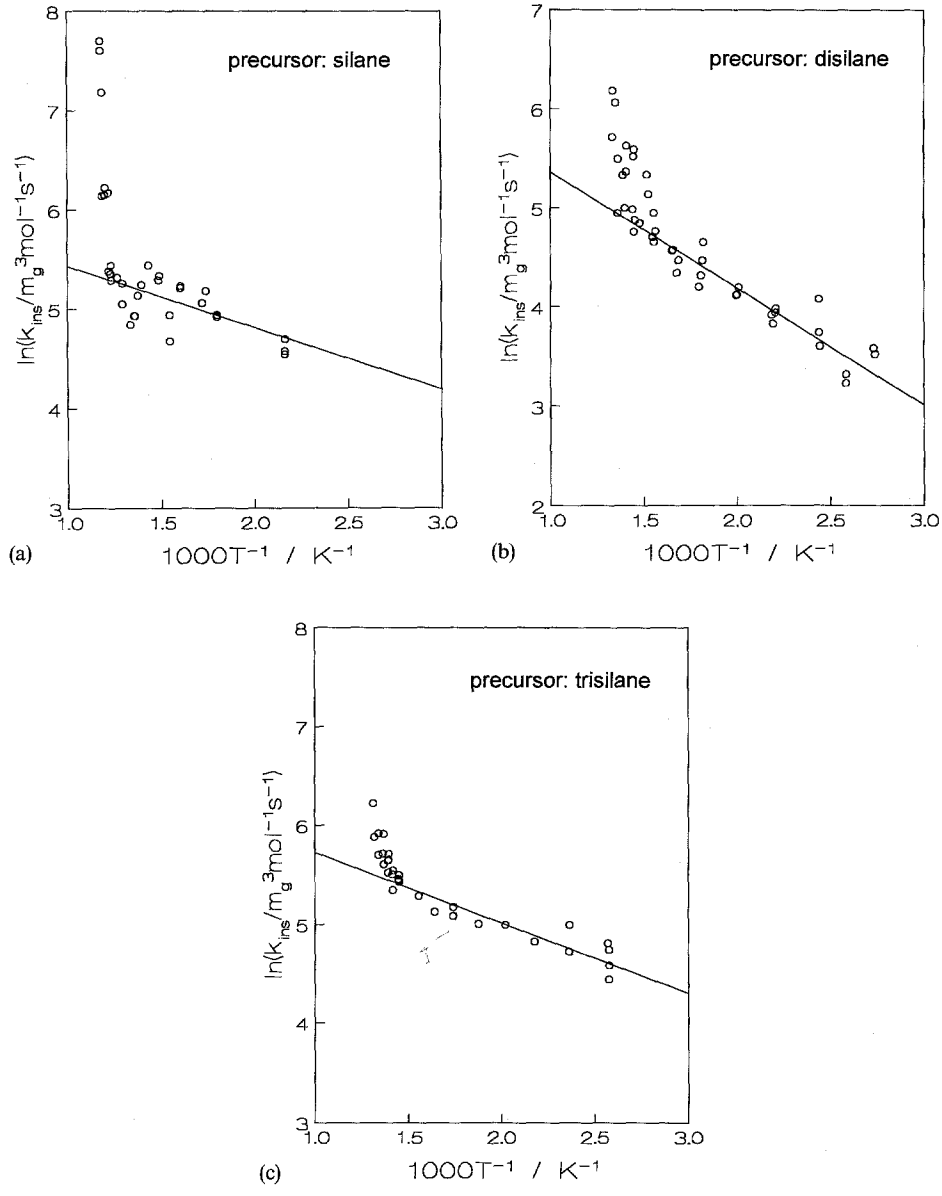

Fig. 8. Arrhenius diagram of the adsorption/insertion rate coefficient of (a) SiH_4, (b) Si_2H_6 and (c) Si_3H_8, applying to the low-temperature region.

lane and trisilane as obtained by regression of the above-mentioned response signals. In both cases two temperature regimes can be distinguished, with a transition for disilane at 650 K and for trisilane at 710 K. For all three silanes the significance of the global regression of the response signals in the high-temperature region is smaller than in the low-temperature region as expressed by means of the F ratio. This also points to a change in mechanism.

Table 2 lists the Arrhenius parameters with approximate individual 95% confidence intervals obtained by regression of the adsorption/insertion

Table 2
Estimates with approximate individual 95% confidence intervals of the Arrhenius parameters associated with the adsorption/insertion reactions of SiH_4, Si_2H_6 and Si_3H_8 on polycrystalline silicon at low temperatures

Species	A (m_g^3 mol^{-1} s^{-1})	E_a (kJ mol^{-1})
SiH_4	424 ± 188	5.14 ± 2.52
Si_2H_6	693 ± 274	9.77 ± 1.84
Si_3H_8	627 ± 141	5.92 ± 1.08

Table 3
Estimates with approximate individual 95% confidence intervals of the standard activation entropies associated with the insertion reactions of SiH_4, Si_2H_6 and Si_3H_8 into surface hydrogen bonds; standard states: 1 atm, $\theta^{\neq} = 0.5$

Species	$\Delta^{\neq}S^0$ (J mol^{-1} K^{-1})
SiH_4	-192 ± 4
Si_2H_6	-186 ± 4
Si_3H_8	-187 ± 2

rate coefficients of silane, disilane and trisilane in the low temperature regions.

Similar to the insertion reaction of silane given above, a gas-phase reaction between silane and silylene giving silylsilylene and hydrogen is described by Ho et al. [30] with a slightly larger activation energy of 24.2 kJ mol^{-1} as compared to 5.1 kJ mol^{-1} estimated here. Indeed, even at temperatures as low as 462 K, small amounts of hydrogen were detected in the present work during the adsorption of silane.

As mentioned in Section 2, considerable temperature gradients exist in the axial direction of the microreactor. The model equations given above do not provide in such gradients. Nevertheless, the assumption concerning isothermicity is quite plausible as the adsorption processes of all three silanes prove to be only slightly, activated as shown in Table 2.

Transition-state theory yields the following expression for the adsorption/insertion rate coefficient k_{ins} in units of atm^{-1} s^{-1}:

$$k_{ins} = \frac{kT}{h} \exp\left(\frac{\Delta^{\neq}S^0}{R} - \frac{\Delta^{\neq}H^0}{RT}\right), \qquad (10)$$

with $\Delta^{\neq}S^0$ and $\Delta^{\neq}H^0$ denoting the standard activation entropy and enthalpy. Table 3 lists the standard activation entropies with approximate individual 95% confidence intervals obtained by regression of the adsorption/insertion rate coefficients of silane, disilane and trisilane in the low-temperature regions.

No literature data on standard activation entropies for the adsorption of silanes exist. Upon adsorption, however, the silanes will lose their translational and at least a part of their external rotational entropy. By means of statistical thermodynamics it can be calculated that at the mean temperature of the experiments the values for the standard translational entropy amount to 168 J mol^{-1} K^{-1} for silane, 171 J mol^{-1} K^{-1} for disilane, and 178 J mol^{-1} K^{-1} for trisilane. For the external rotational entropy, values of 59 J mol^{-1} K^{-1} for silane, 89 J mol^{-1} K^{-1} for disilane, and 121 J mol^{-1} K^{-1} for trisilane can be calculated. The standard activation entropies listed in Table 3 and obtained by regression of the experimental data agree reasonably well with the theoretical expectations, since on adsorption the translational entropy as well as a part of the rotational entropy of the adsorbing species will be lost.

4.3. *Silane adsorption at T>820 K*

In Section 4.2 the slow adsorption of silane via insertion, occuring at low temperatures, was discussed. At 820 K a distinct change is observed in the silane conversion and in the activation energy of the reaction. This seems to correspond to a change in mechanism, as from this temperature the regression of the silane response from Eqs. (9) and (2)–(5) for the low-temperature regime is rather poor.

Kinetic modelling studies of polycrystalline silicon growth [13,27], as well as fundamental studies of silicon hydride chemistry on Si(001) and Si(111) surfaces [31], provide the basis for a possible reaction sequence describing silicon deposition from silane at temperatures higher than 820 K. This reaction sequence is shown in Table 4, where * means a vacant site at the silicon surface, i.e. a dangling bond.

The dissociative adsorption of silane (S1) here is considered irreversible. Alternatively, using

Table 4
Elementary reactions considered on the silicon surface (S1)–(S6) and global reactions (α,β)

	σ_α	σ_β	
(S1) $SiH_4 + 2^* \rightarrow SiH_3^* + H^*$	1		
(S2) $SiH_3^* + {}^* \rightarrow SiH_2^* + H^*$	1		
(S3) $SiH_2^* + {}^* \rightarrow SiH^* + H^*$	1		
(S4) $SiH^* \rightarrow Si(s) + H^*$	1		
$SiH_4 + 4^* \rightarrow Si(s) + 4H^*$		1	(α)
(S5) $2H^* \rightleftarrows H_2 + 2^*$		2	
$SiH_4 \rightarrow Si(s) + 2H_2$			(β)

single-site non-dissociative adsorption of silane instead of reaction S1, no good fit to the experimental data could be obtained. Hydrogen desorption is accounted for through reaction S5. As discussed by various authors [3,4,24–26], the desorption reaction is of first order in hydrogen adatom coverage on Si(001). Also, in studies on the growth mechanism of polycrystalline silicon under LPCVD conditions [13,27] a first-order desorption reaction for hydrogen is found. Here, reaction S5 is taken as being irreversible because of the low hydrogen pressures during a TAP experiment. In addition, surface diffusion is considered to be very fast as compared to hydrogen abstraction [15].

In the reaction sequence shown in Table 4, only the silane adsorption reaction (S1) and the desorption reaction of hydrogen adatoms (S5) are considered to be kinetically significant. Consequently, decomposition of SiH_3^* (S2) as well as of SiH_2^* (S3) and of SiH* (S4) are assumed to proceed potentially fast as compared to the SiH_4 adsorption (S1). This implies that H* is the only kinetically significant surface species. It should be noted that the term in the balances reflecting the slow adsorption process via insertion which is dominating at low temperature, and which can be written in the terminology of Table 4 as

$$^*H + SiH_4 \rightarrow Si(s) - H + 2H_2,$$

is now omitted. This adsorption process will have only a small contribution to the overall adsorption process at high temperatures.

With the additional assumptions given earlier, the following mass balances for silane and vacant surface sites apply

$$\epsilon \frac{\partial C_{SiH_4}}{\partial t} = D_{K,eff,SiH_4} \frac{\partial^2 C_{SiH_4}}{\partial x^2} - a_v L_t k_a (1-\theta^0_{H*})^2 \hat{\theta}^2 C_{SiH_4}, \quad (11)$$

$$\frac{\partial \hat{\theta}}{\partial t} = -4k_a(1-\theta^0_{H*})\hat{\theta}^2 C_{SiH_4} + 2k_d \frac{[1-\hat{\theta}(1-\theta^0_{H*})]}{(1-\theta^0_{H*})}, \quad (12)$$

with:

$$\hat{\theta} = \frac{\theta_*}{1-\theta^0_{H*}}, \quad (13)$$

and subjected to the following initial and boundary conditions

$$t = t_0 \wedge 0 \leq x \leq L \quad C_{SiH_4} = \frac{N_{p,SiH_4}}{\epsilon A_s} \delta_x, \quad (14)$$

$$t = t_0 \wedge 0 \leq x \leq L \quad \hat{\theta} = 1, \quad (15)$$

$$t \geq t_0 \wedge x = 0 \quad \frac{\partial C_{SiH_4}}{\partial x} = 0, \quad (16)$$

and

$$t \geq t_0 \wedge x = L \quad C_{SiH_4} = 0. \quad (17)$$

Here k_d is the first-order rate coefficient for the desorption of surface hydrogen. Note that contrary to Eq. (9), in Eq. (11) the production term explicitly shows a dependency on the fraction of vacant sites. At temperatures above 820 K it is assumed that the adsorption takes place at a dual vacant surface site. The coverage of these sites will be significantly larger than zero at the temperatures used, but will certainly not amount to one. Therefore the amount of adsorption sites in the reactor will be of the same order of magnitude as the pulse size and changes in it will not be negligible. Hence, a continuity equation for the vacant sites (Eq. (12)) is also considered. The initial condition for the fraction of free surface sites is determined by the fractional surface coverage of H*, θ^0_{H*}, at the beginning of each transient. The fraction of vacant sites at the beginning of the experiment equals $1-\theta^0_{H*}$, with θ^0_{H*} the coverage of hydrogen at $t = t_o$. The mass balances of silane and vacant sites

can then be written in terms of a normalized fraction of vacant sites as defined in Eq. (13). Here $\hat{\theta}$ is the fraction of vacant sites on the available part of the surface at $t=t_o$.

Parameter estimates for single-pulse experiments at 844 and 849 K were obtained using the above continuity equations. From these the value of k_d could not be estimated to be significantly different from zero, indicating that the characteristic time for hydrogen desorption, even at these temperatures, is too large to be within the window of measurable time scales in the present TAP configuration. Therefore, the term corresponding to hydrogen desorption was skipped in Eq. (12). It is thus assumed that hydrogen, adsorbed at the surface at $t=t_0$, will stay there during the experiment. Both above-mentioned single-pulse experiments at 844 and 849 K with a binary gas mixture of 20% argon in silane are regressed using Eqs. (11)–(17), thereby omitting the term in the right-hand side of Eq. (12) corresponding to hydrogen desorption. The adsorption rate coefficient k_a and the initial fraction of bare surface $(1-\theta^0_{H*})$ are estimated using the parameter estimation methods discussed in Section 2.4. Very good agreement between experiment and model is observed for both experiments. The estimates, however, for k_a and $(1-\theta^0_{H*})$ are, as expected, strongly correlated with a binary correlation coefficient up to 0.994, implying that the significance of the obtained values for k_a and $(1-\theta^0_{H*})$ is rather low. It is therefore necessary to have an independent estimate of one of these parameters in order to obtain a significant estimate of the other.

Kinetic modelling of steady-state experiments of polysilicon deposition in a gradientless reactor [13] gives a value for the sticking probability of SiH_4 on a empty surface of 2.3×10^{-3}. From this, values for k_a equal to 37 665 $m_g^3\ mol^{-1}\ s^{-1}$ at 844 K and to 37 776 $m_g^3\ mol^{-1}\ s^{-1}$ at 849 K can be calculated. Using the latter values for k_a in the modelling of the transient responses, excellent agreement between the experimental response and the response calculated with Eqs. (11)–(17) is obtained as can be seen in Fig. 2 (curve B) for $T=$ 849 K. For both experiments the zero time found by regression equals about 1.2 ms, the same value also found for the experiments discussed in the previous sections. The initial bare fraction of the surface, $(1-\theta^0_{H*})$, equals 0.236 ± 0.002 at 844 K and 0.316 ± 0.001 at 849 K.

Reconsidering the qualitative results given in Section 3.1, it now is clear why the multipulse experiments in the high-temperature region are difficult to reproduce, and why the conversion of silane increases strongly from about $T=820$ K onwards. Obviously the conversion of silane is a strong function of the initial state of the surface, and a small change in initial hydrogen coverage θ^0_{H*} will lead to a large change in silane conversion. As all single-pulse experiments are performed using signal averaging after a series of pulses to obtain a stable response signal, it is difficult to tell the exact amount of vacant sites in the beginning of the single-pulse sequence. However, the values for the fraction $(1-\theta^0_{H*})$ found from the regression analysis of the experimental data seem quite reasonable taking into account a characteristic time for desorption of hydrogen of about 1 s and a time between pulses in the signal averaging mode also of 1 s.

5. Conclusions

The adsorption of silanes at polycrystalline silicon was studied by means of temporal analysis of products in the temperature range 300–1000 K. Qualitative experiments with silane, disilane and trisilane revealed that at low temperatures, slow adsorption processes are operative. The reactivity for the three silanes towards adsorption on polysilicon is about equal, whereas the apparent activation energies are quite low and more or less equal to each other. However, at roughly 650 K, a transition is observed towards a faster mode of adsorption. The adsorption of the higher silanes above their respective transition temperatures is accompanied by silane formation. For all three silanes, the apparent activation energy for adsorption is strongly increased in this temperature range.

Quantitative experiments with inert gases showed that the gas transport through the reactor could be described by Knudsen diffusion. The same transport mode is used for the quantitative modelling of the transient responses of silane, disilane

and trisilane. An adequate description of the adsorption of the silanes in the temperature ranges below the respective transition temperatures is provided by an insertion reaction of SiH_4, Si_2H_6 or Si_3H_8 into surface hydrogen bonds followed by fast decomposition of the formed species into Si–H moieties, which can act as new adsorption centres. Silane adsorption above the transition temperature of 820 K could be described very well with a mechanism consisting of dual-site adsorption of silane onto vacant surface sites, subsequent fast decomposition of the formed surface hydride species, and desorption of hydrogen. This mechanism is similar to that used to describe polycrystalline silicon growth from silane [13]. The TAP experiments give strong evidence for the validity of the latter.

References

[1] S.M. Gates, C.M. Greenlief and D.B. Beach, J. Chem. Phys. 93 (1990) 7493.
[2] S.K. Kulkarni, S.M. Gates, C.M. Greenlief and H.H. Sawin, Surf. Sci. 239 (1990) 26.
[3] K. Sinniah, M.G. Sherman, L.D. Lewis, W.H. Weinberg, J.T. Yates, Jr. and K.C. Janda, Phys. Rev. Lett. 62 (1989) 567.
[4] M.L. Wise, B.G. Koehler, P. Gupta, P.A. Coon and S.M. George, Surf. Sci. 258 (1991) 166.
[5] M.K. Farnaam and D.R. Olander, Surf. Sci. 145 (1984) 390.
[6] S.K. Kulkarni, S.M. Gates, B.A. Scott and H.H. Sawin, Surf. Sci. 239 (1990) 13.
[7] K. Werner, S. Butzke, S. Radelaar and P. Balk, J. Cryst. Growth 136 (1994) 322.
[8] R.J. Buss, P. Ho, W.G. Breiland and M.E. Coltrin, J. Appl. Phys. 63 (1988) 2808.
[9] J.T. Gleaves, J.R. Ebner and T.C. Kuechler, Catal. Rev. Sci. Eng. 30 (1988) 49.
[10] G.L. Svoboda, J.T. Gleaves and P.L. Mills, Ind. Eng. Chem. Res. 31 (1992) 19.
[11] D.W. Marquardt, J. Soc. Ind. Appl. Math. 11 (1963) 431.
[12] N.R. Draper and H. Smith, Applied Regression Analysis (Wiley, New York, 1966).
[13] W.L.M. Weerts, PhD Thesis, Eindhoven, 1995.
[14] S.M. Gates, C.M. Greenlief, D.B. Beach and R.R. Kunz, Chem. Phys. Lett. 154 (1989) 505.
[15] S.M. Gates and S.K. Kulkarni, Appl. Phys. Lett. 58 (1991) 2963.
[16] S.M. Gates, Surf. Sci. 195 (1988) 307.
[17] J.P. Huinink, PhD Thesis, Eindhoven, 1995.
[18] D.S. Zou, M.P. Dudukovic and P.L. Mills, J. Catal. 145 (1994) 683.
[19] NAG Ltd, Fortran Library Manual, #15 (Wilkinson House, Oxford, 1991).
[20] B.D. Eldridge and L.F. Brown, AIChE J. 22 (1976) 942.
[21] P. Clausing, Physica 9 (1929) 65.
[22] D.G. Coronell and K.F. Jensen, J. Electrochem. Soc. 139 (1992) 2264.
[23] M.P. D'Evelyn, Y.L. Yang and L.F. Sutcu, J. Chem. Phys. 96 (1992) 852.
[24] K.W. Kolasinski, S.F. Shane and R.N. Zare, J. Chem. Phys. 95 (1991) 5482.
[25] J.J. Boland, J. Vac. Sci. Technol. A 10 (1992) 2458.
[26] M.C. Flowers, N.B.H. Jonathan, Y. Liu and A. Morris, J. Chem. Phys. 99 (1993) 7038.
[27] J. Holleman and J.F. Verweij, J. Electrochem. Soc. 140 (1993) 2089.
[28] H. Kanoh, O. Sugirura and M. Matsumura, Jpn. J. Appl. Phys. 32 (1993) 2613.
[29] S.M. Gates and S.K. Kulkarni, Appl. Phys. Lett. 60 (1992) 53.
[30] P. Ho, M.E. Coltrin and W.G. Breiland, J. Phys. Chem. 98 (1994) 10138.
[31] J.N. Jasinski and S.M. Gates, Acc. Chem. Res. 24 (1991) 9.